ISIJ International, Vol. 56 (2016), No. 5, pp. 868–874

Strain Rate and Temperature Insensitiveness of Notch-bend Strength for High Si Ductile Cast Iron

Tomohiro IKEDA,[1)]* Takuo UMETANI,[1)] Nobuhiro KAI,[1)] Nao-Aki NODA[2)] and Yoshikazu SANO[2)]

1) HINODE, Ltd., Azaiwasaki, Miyaki-cho, Miyaki-gun, Saga, 849-0101 Japan.
2) Kyushu Institute of Technology, Sensui-cho, Tobata-ku, Kitakyushu, Fukuoka, 804-8550 Japan.

(*Received on September 4, 2015; accepted on January 8, 2016; J-STAGE Advance published date: March 31, 2016*)

The notch-bend strength ($\sigma_{b,max}$) was investigated for High Si Solid Solution Strengthened Ferritic Ductile Cast Iron (EN-GJS-500-14) with varying the strain rate at room temperature. The notch-bend strength was also compared with the conventional ferrite-pearlite type ductile cast iron JIS-FCD500 and JIS-FCD700. Then, the application of the high Si ductile cast iron to wide industrial fields was discussed. Dynamic three-point bending tests were conducted on Charpy V-notch specimens in the range of stroke speed, 10^{-3}～10^{2} mm/s, at −20～22°C. The load-displacement curve for ductile fractured specimens shows that the load (P) steeply increases to the peak value (P_{max}; about 10 kN) and then decreases, similar to that in the case of instrumented Charpy impact test. Even though the absorbed energy of fracture process was in the lower shelf region, the notch-bend strength did not decrease with increasing the strain rate as far as the fracture origin is ductile. It was found that the notch-bend strength is insensitive to the strain rate. The notch-bend strength ($\sigma_{b,max}$) of high Si ductile cast iron at −20°C was still equal to that at 22°C, indicating $\sigma_{b,max}$ is insensitive to the temperature as well as the strain rate. High Si ductile cast iron EN-GJS-500-14 and the conventional ductile cast irons JIS-FCD500 and JIS-FCD700 show nearly the same lowest $\sigma_{b,max}$ in the range of strain rate, 1.5×10^{-4}～2.0×10^{0}s^{-1} at −20°C. Therefore, we think that the high Si ductile cast iron has wide industrial application potentiality.

KEY WORDS: cast iron; high silicon; strength; strain rate; temperature.

1. Introduction

Conventional ferrite-pearlite type ductile cast irons are widely used as structural members for automobile, railway vehicle, machine tool, and so on. These cast irons have a broad range of mechanical properties, and in some cases they have replaced cast steel and forging products.[1)] Usually, the required strength can be obtained by controlling the ferrite-pearlite ratio in the matrix. Typically, ferritic ductile cast iron has high elongation and low tensile strength, which is approximately 350 MPa, while pearlitic ductile cast iron has low elongation and high tensile strength ranging over 800 MPa. The greatest amount of research has been conducted on the effects of ferritic, pearlitic or ferritic–pearlitic matrices on the mechanical property of ductile cast iron.[1,2)]

Meanwhile, in recent years, High Si Solid Solution Strengthened Ferritic Ductile Cast Iron (high Si ductile cast iron) has been attracting attention in Europe.[3–5)] This material has been already standardized in EN 1563 with the tensile strength in the range of 450–600 MPa at the Si content in the range of 3.0–4.3%.[6)] The high Si ductile cast iron can provide fully ferritic matrix even at the smaller cross-section because of higher silicon content than normal 2.0–2.7%Si. Therefore, the high Si cast iron has smaller section sensitivity. Furthermore, elongation and fatigue strength of the high Si ductile cast iron are higher than that of a similar strength level of conventional ferrite-pearlite ductile cast iron.[7)] Those advantages indicate wide industrial application potentiality of this material. Application of the high Si ductile cast iron has been investigated at room temperature in Europe.[3)]

On the contrary, it is known that higher Si content raises the ductile-brittle transition temperature in Charpy impact test.[8–10)] Therefore, one may afraid that Charpy absorbed energy of high Si ductile cast iron is not enough at room temperature. This is one of the reasons why this material has not been widely used in wide industrial field yet. Charpy impact test is sometimes not suitable for evaluating the impact strength because the impact speed does not correspond to the real products failure. The toughness of ductile cast iron strongly depends on strain rate as well as temperature. However, it is difficult to control the pendulum impact speed in Charpy impact test. Therefore, for example, one of the authors studied high-speed tensile testing with varying tensile speed to investigate the impact property in engineering plastics.[11–13)] In addition, it should be noted that Charpy absorbed energy has not been directly used in mechanical design strength differently from commonly used tensile strength and yield strength. To design the casting members

* Corresponding author: E-mail: t_ikeda@hinodesuido.co.jp
DOI: http://dx.doi.org/10.2355/isijinternational.ISIJINT-2015-516

in structures, it is necessary to know the effect of strain rate and temperature on the strength.

In this study, the dynamic three-point bending tests will be conducted controlling the stroke speed=10^{-3}~10^{2} mm/s at −20~22°C for Charpy V-notch specimens. Then, the notch-bend strength will be discussed with varying the strain rate at 22°C and −20°C. Industrial application potentiality of high Si ductile cast iron will be examined in comparison with conventional ferrite-pearlite type ductile cast irons.

2. Experimental Procedures

2.1. Preparation of Cast Specimen

High Si ductile cast iron (SSFDI500) is considered in comparison with conventional ductile cast irons of tensile strength 500 MPa (JIS-FCD500) and 700 MPa (JIS-FCD700). **Table 1** shows their chemical compositions. In this alloy, Si content is designed about twice of that of standard cast iron, and C is slightly reduced depending on Si composition. As a pearlite former element, Cu is added to JIS-FCD500 and JIS-FCD700 to distribute an appropriate amount of pearlite in the matrix. Type-B Y-shaped blocks (JIS-G 5502)[14] shown in **Fig. 1** are cast in sand molds.

Table 1. Chemical compositions of as cast specimens (mass%).

Material	C	Si	Mn	P	S	Cu	Mg
SSFDI500	3.20	3.72	0.32	0.022	0.008	0.02	0.038
JIS-FCD500	3.63	2.02	0.42	0.020	0.011	0.26	0.029
JIS-FCD700	3.64	2.14	0.42	0.022	0.003	0.38	0.039

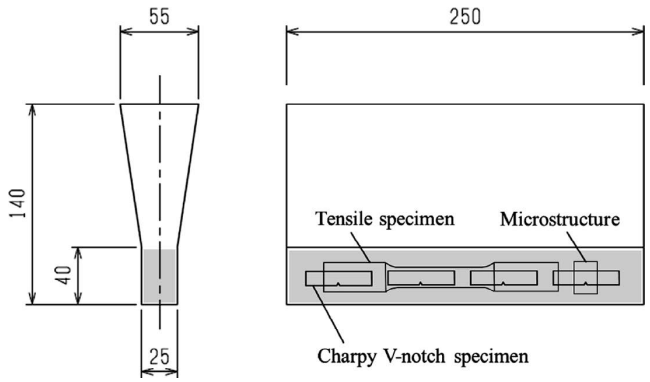

Fig. 1. Schematic view of Y-sharped block.

All test specimens, such as JIS No. 4 test pieces, are taken from the as cast Y-shaped blocks of the highlighted sections in gray whose dimensions are 40×25×250 mm in Fig. 1. **Figure 2** shows typical microstructures of test specimens. SSFDI500 has fully ferritic matrix although conventional ductile cast irons are composed of ferritic-pearlitic matrix. JIS-FCD500 has pearlite ratio of 52% and JIS-FCD700 has pearlite ratio of 87%, respectively. **Table 2** summarized graphite structures of test specimens based on the analysis according to JIS-G5502, and it is seen that every material has nearly the same graphite structures. As shown in Table 2, nodule count are about 200, average nodule diameter is around 28 μm, nodularity is around 98% and graphite area fraction is from 10 to 11%. **Table 3** shows the tensile property of test specimens based on JIS No. 4 test piece whose diameter=14 mm and gage length=50 mm.[15] The test procedure meets JIS-Z 2241 standard. It is seen that tensile strength of JIS-FCD500 is similar to that of SSFDI500, whereas 0.2% proof stress of JIS-FCD700 is similar to that of SSFDI500.

2.2. Charpy Impact Test

Figure 3 shows Charpy V-notch specimen dimensions. Configuration of specimen setting is also shown in this figure (b). The impact test is performed using a Charpy impact machine with 300 J maximum energy capacity (Shimadzu: JIS 300J) at the condition of the impact

Table 2. Graphite structures of as cast specimens.

Material	Nodule count (mm^{-2})	Average nodule diameter (μm)	Nodularity (%)	Graphite area fraction (%)
SSFDI500	192	28.1	97.7	10.6
JIS-FCD500	174	30.0	97.9	11.7
JIS-FCD700	202	27.3	97.5	10.2

Table 3. Tensile properties of test specimens.

Material	σ_B (MPa)	$\sigma_{0.2}$ (MPa)	ε_B(%)
SSFDI500	525	401	21
JIS-FCD500	555	336	13
JIS-FCD700	734	392	10

σ_B: Tensile strength, $\sigma_{0.2}$: 0.2% proof stress, ε_B: Fracture strain

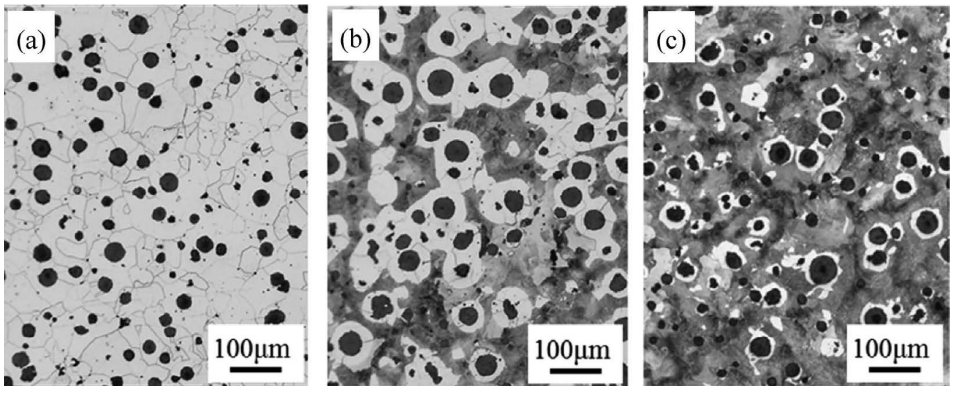

Fig. 2. Microstructures of as cast specimens, SSFDI500 (a), JIS-FCD500 (b), JIS-FCD700 (c).

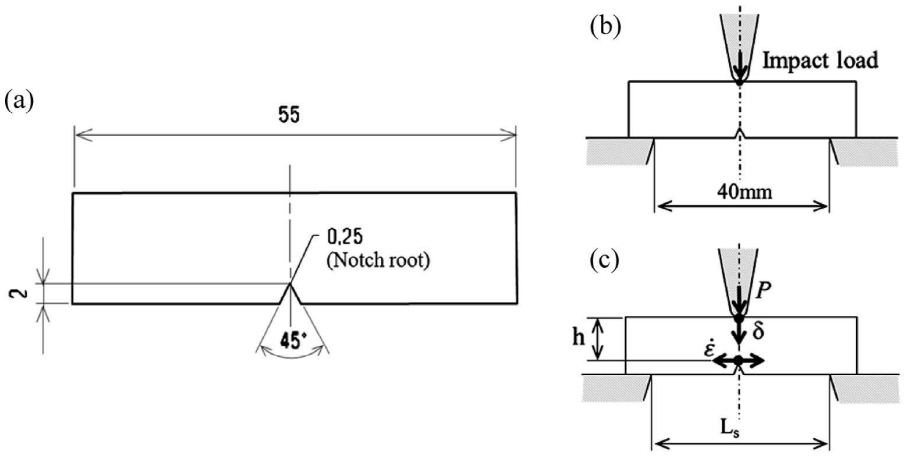

Fig. 3. V-notch specimen (JIS-Z 2242) (a), the configuration of Charpy impact test (b) and dynamic three-point bending test (c).

speed = 5.18×10^3mm/s. The total absorbed energy in the fracture process E_c is determined by measuring the decrease in motion of the pendulum arm according to JIS-Z2242 standards.[16] The ductile fracture surface ratio f_D is determined macroscopically from microscope photograph for showing the fracture morphology.

2.3. Dynamic Three-point Bending Test

In order to evaluate the brittle and ductile fracture at the wide range of bending speed, dynamic three-point bending test is carried out using V-notch specimen. Test condition was systematically varied in the range of stroke speed, $\upsilon = 10^{-3}$~10^2 mm/s, at −20~22°C by using electrohydraulic servo testing machine (Shimadzu: E100kN). The bending jig whose span length Ls = 40 mm has the same shape and size as the Charpy impact testing machine as shown in Fig. 3(c). The strain rate $\dot{\varepsilon}$ is calculated by using Eq. (1),[17–20] where h = test specimen width, Q = 1.94,[17–19] υ = stroke speed, L_s = span length.

$$\dot{\varepsilon} = 6h\upsilon Q / L_s^2 \quad \text{..... (1)}$$

The total absorbed energy E_t in the fracture process is also obtained from area under the load-displacement curve of the three-point bending test. The fractographic analysis is performed by optical observations and scanning electron microscopy (SEM, Hitachi S-3400N). The ductile fracture surface ratio f_D is determined macroscopically from microscope photograph. SEM observation is also made to reveal the details of fracture morphology especially near V-notch root where the fracture started.

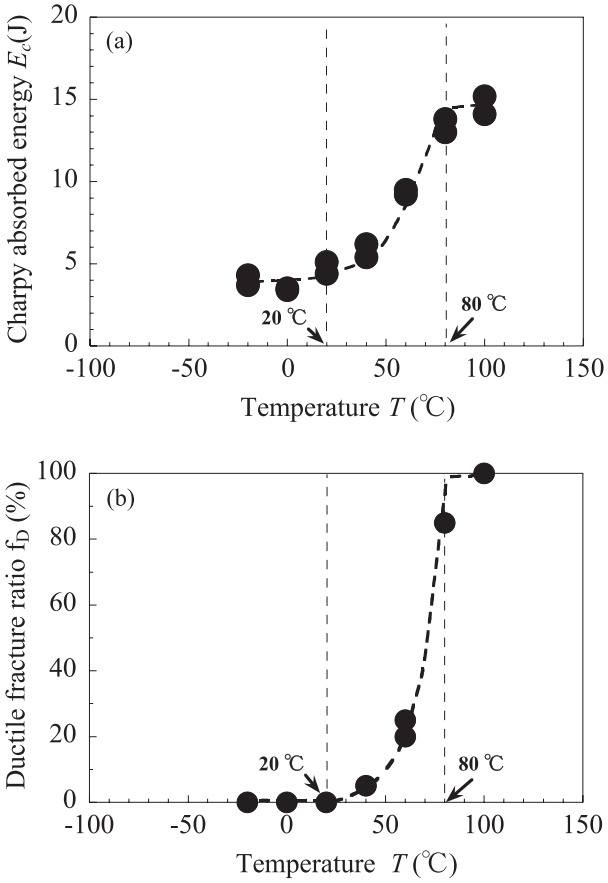

Fig. 4. Results of Charpy impact test for SSFDI500, transition curves of absorbed energy (a) and ductile fracture ratio (b).

3. Results and Discussion

3.1. Charpy Transition Curve

Figure 4 shows temperature dependence of the absorbed energy of V-notch Charpy impact test for SSFDI500. The absorbed energy E_c of 15 J starts dropping at the critical temperature for upper shelf region of 80°C as indicated by the right arrow, and finally reaches to 4 J at 20°C. In Fig. 4(b), ductile fracture ratio f_D starts dropping at the same critical temperature of E_c. Brittle fracture surface appears below this critical temperature, and f_D decreases with the temperature decreasing. From Figs. 4(a), 4(b), a good coincidence can be seen for the transition of E_c and f_D, indicating that the reduction of E_c is caused by ductile-brittle fracture surface transition.

3.2. Absorbed Energy Depending on Strain Rate

From Charpy impact test, SSFDI500 has brittle characteristics around room temperature. However, it is necessary to clarify the strain rate dependence in order to expand a further application. Therefore, the absorbed energy was evaluated in relation with the strain rate. **Figure 5** shows the effect of the strain rate $\dot{\varepsilon}$ on the absorbed energy E_t (a) and f_D (b) of the three-point bending test at 22°C for SSFDI500.

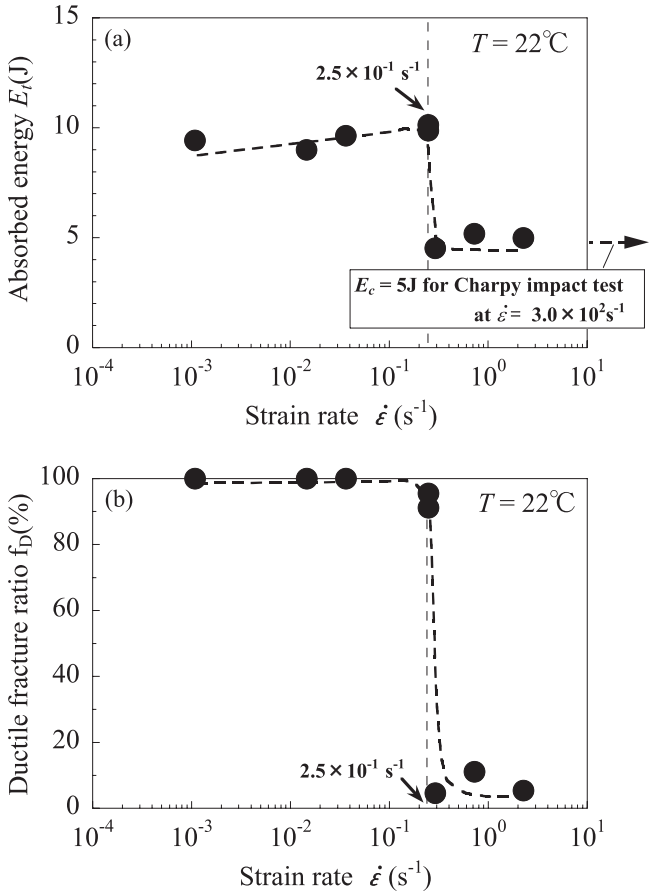

Fig. 5. Effect of strain rate on absorbed energy (a) and ductile fracture surface ratio (b) at temperature T=22°C for SSFDI500.

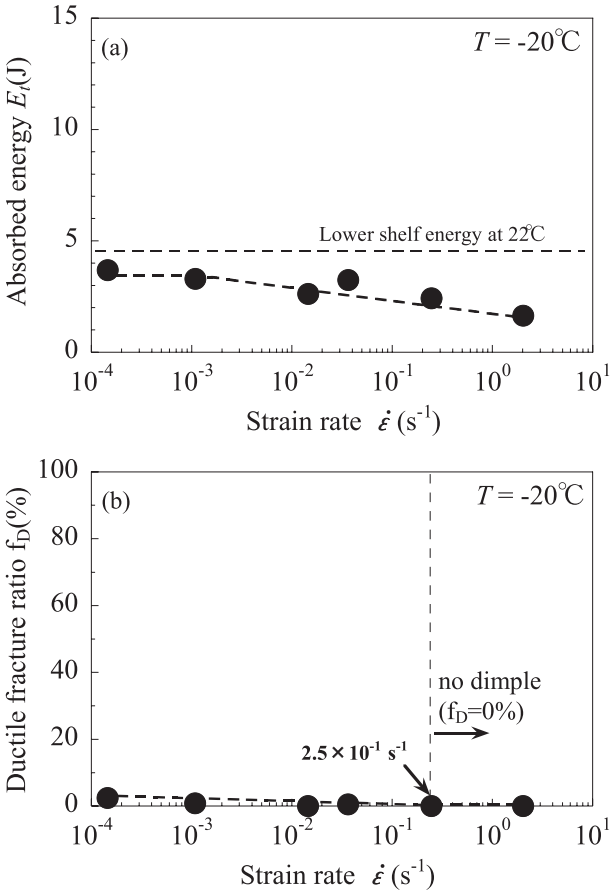

Fig. 6. Effect of strain rate on absorbed energy (a) and ductile fracture surface ratio (b) at temperature T=−20°C for SSFDI500.

The upper shelf region is recognized even at 22°C, room temperature. In Fig. 5(a), the absorbed energy starts dropping from 10 to 5 J at $\dot{\varepsilon}$ of 2.5×10^{-1}s^{-1} as indicated by the arrow and brittle fracture surface appears above this critical strain rate. Similar to the results of Charpy impact test a good coincidence can be seen for the transition of E_t and f_D, and it may be concluded that the reduction of E_t is caused by ductile-brittle fracture surface transition by increasing $\dot{\varepsilon}$. Figure 5(a) also indicates that the result of E_c is 5 J for Charpy impact test whose strain rate can be estimated by Eq. (1) as about 3.0×10^{2}s^{-1} at the beginning of fracture process.

Figure 6 shows the results of lower test temperature −20°C for $\dot{\varepsilon}$ on E_t (a) and f_D (b) on SSFDI500. It is seen that all E_t at −20°C is smaller than the lower shelf energy at 22°C in Fig. 5(a), which indicates that the lower holding temperature would decrease the critical strain rate of ductile-brittle transition.

3.3. Notch-bend Strength Insensitive to Strain Rate

3.3.1. Notch-bend Strength at 22°C with Ductile Behavior

Figure 7 shows load-displacement curves of the three-point bending tests under different $\dot{\varepsilon}$ at 22°C for SSFDI500. Here, P_{max} is the maximum load, and the maximum displacement δ_{max} is defined as the displacement at the final fracture as indicated by the cross mark in Fig. 7. It is seen that δ_{max} decreases with increasing $\dot{\varepsilon}$, and therefore, E_t decrease with increasing $\dot{\varepsilon}$ in Fig. 5(a). On the contrary, in Fig. 7, P_{max} slightly increases with increasing $\dot{\varepsilon}$. It should be noted that fracture does not happen if real load is smaller than P_{max}.

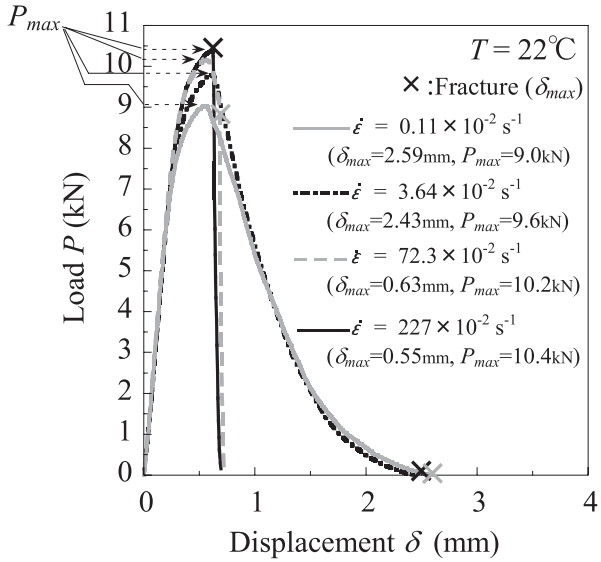

Fig. 7. Variation in load-displacement curves of the three-point bending test with strain rate at temperature T=22°C for SSFDI500.

Figure 8 shows the relationship between $\sigma_{b,max}$ and $\dot{\varepsilon}$ at 22°C for SSFDI 500. The notch-bend strength $\sigma_{b,max}$ was defined from P_{max} as shown in Eq. (2),[21,22] without considering notch stress concentration. Here, P_{max}=maximum load, L_s=span length, b=test specimen thickness, h=test specimen width.

$$\sigma_{b,max} = 3P_{max}L_s / 2bh^2 \quad \text{..... (2)}$$

For comparison, the relationship between E_t and $\dot{\varepsilon}$ shown in Fig. 5(a) is also plotted in Fig. 8. The notch-bend strength $\sigma_{b,max}$ of 850 MPa, does not decrease insensitive to $\dot{\varepsilon}$ even though when E_t is in the lower shelf region above $\dot{\varepsilon}$ of $2.5\times10^{-1}s^{-1}$.

Figure 9 shows the fracture surface at $\dot{\varepsilon}$ of $72.3\times10^{-2}s^{-1}$ specimen, and figure (b) and (c) indicate SEM images of fracture surface for black and white areas in Fig. 9(a). It is seen that the black area is composed of dimple patterns characterizing ductile fracture. On the other hand, white area is composed of cleavage fracture surface characterizing brittle fracture. **Figure 10** shows SEM image at the notch root of $227\times10^{-2}s^{-1}$ specimen. Even though macroscopic observation shows that almost no ductile fracture surface is included in Fig. 10(a), microscopic SEM observation shows that a slight amount of dimple patterns observed near the notch root in Figure (b). This slight amount of dimple area is probably caused by the initial stage of ductile fracture.

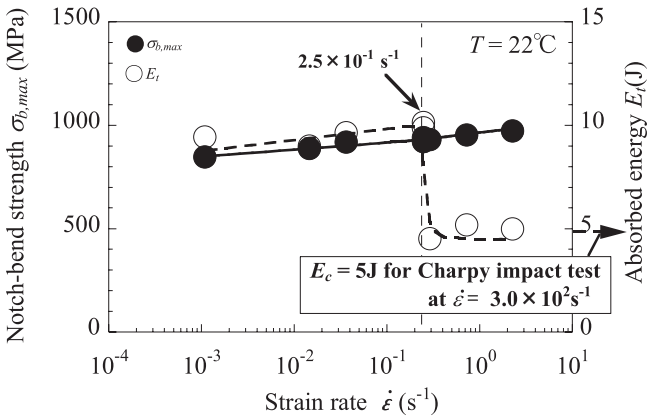

Fig. 8. Effect of strain rate on the notch-bend strength at temperature T=22°C for SSFDI500.

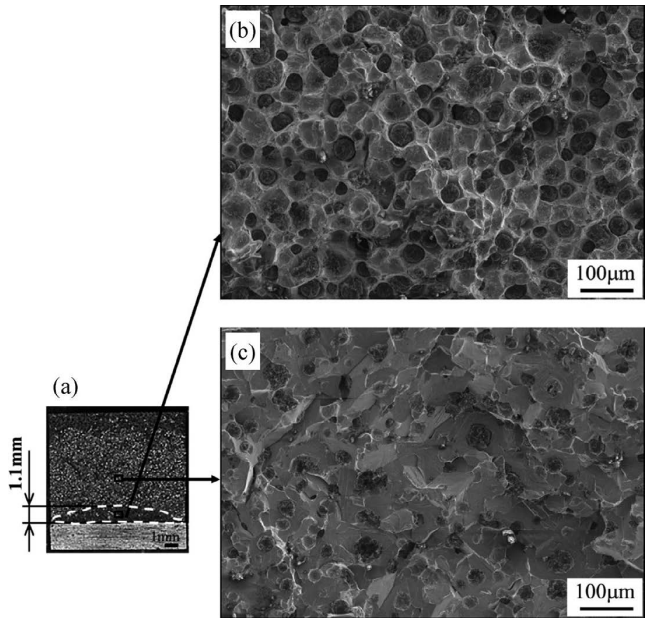

Fig. 9. Fracture surface of specimen at $\dot{\varepsilon}=72.3\times10^{-2}s^{-1}$ (a) and the high magnified images of ductile fracture area (b) and brittle fracture area (c).

Several researchers observed that microcrack initiation at the notch root under three point bending test.[23–24] It was reported that when ductile fracture occurs, an approximately 50 μm microcrack initiates at the notch root.[21] At the same time, separation of spheroidal graphite and ferritic matrix was confirmed.[23] Then, the microcrack extends to the macrocrack larger than 0.1 mm at the vicinity of the maximum load, and propagates.[23] When brittle fracture occurs, a microcrack propagates rapidly almost at the same time of crack initiation.[24] Therefore, it is conjectured that brittle fracture occurs just after forming the slight dimple ductile fracture at the notch root at high strain rate. In this experiment at 22°C, the dimple pattern is always observed at every notch root. Hence, the $\sigma_{b,max}$ keeps increasing with increasing $\dot{\varepsilon}$ as far as the fracture origin is ductile. Figures 9(a) and 10(b) also indicate the ductile layer at notch root. The ductile layer has depth of about 1 mm at Fig. 9(a), and about 0.3 mm in Fig. 10(b). From Fig. 7, δ_{max} is 0.63 mm for Fig. 9(a) specimen, and 0.55 mm for Fig. 10(b) specimen. The ductile layer depth may increases with increasing δ_{max} although the amount of data is not enough.

3.3.2. Notch-bend Strength at −20°C with Brittle Behavior

Figure 11 shows load-displacement curves of the three-point bending test under different $\dot{\varepsilon}$ at the lower temperature

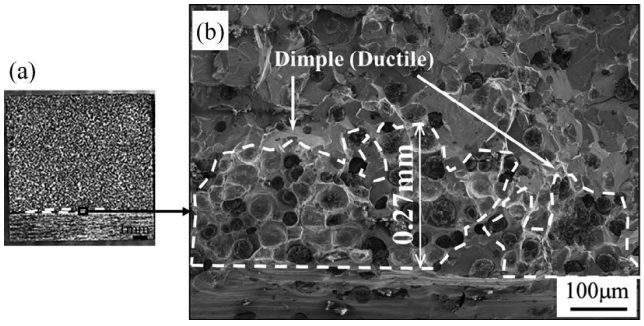

Fig. 10. Fracture surface of specimen at $\dot{\varepsilon}=227\times10^{-2}s^{-1}$ (a) and the high magnified image at vicinity of notch root (b).

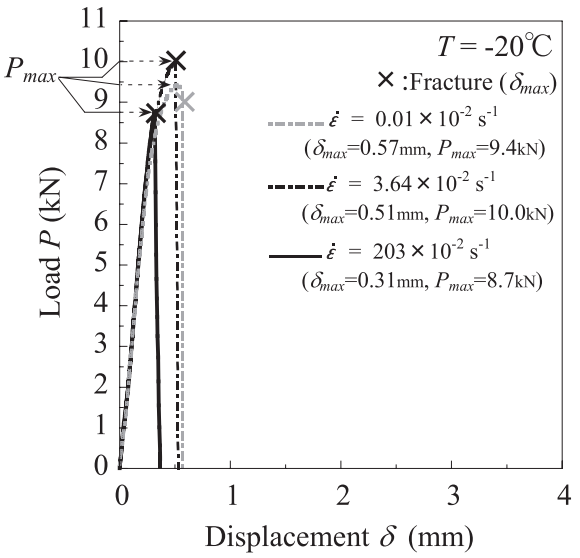

Fig. 11. Variation in load-displacement curves of the three-point bending test with strain rate at temperature T=−20°C for SSFDI500.

−20°C for SSFDI500. It is seen that $\sigma_{b,max}$ decreases with increase in $\dot{\varepsilon}$, at −20°C, this phenomena is different from that at 22°C. Therefore, $\sigma_{b,max}$ was compared with that of 22°C. **Figure 12**(a) shows the relationship between $\sigma_{b,max}$ and $\dot{\varepsilon}$ at the lower temperature −20°C for SSFDI 500. For comparison, the relationship between E_t and $\dot{\varepsilon}$ in Fig. 6(a) is put again in Fig. 12(b). Results at 22°C in Figs. 8 and 5(a) are also plotted in Figs. 12(a) and 12(b). In Fig. 12(a), lowest $\sigma_{b,max}$ at −20°C is still almost the same value of lowest $\sigma_{b,max}$ of 22°C. In other words, $\sigma_{b,max}$ is insensitive to the temperature as well as $\dot{\varepsilon}$. On the contrary, from Fig. 12(b), it is seen that E_t decreases over $\dot{\varepsilon}=2.5\times10^{-1}\mathrm{s}^{-1}$ at 22°C. High Si ductile cast iron has a wide industrial application potentiality because the notch-bend strength insensitiveness to $\dot{\varepsilon}$ and temperature although the absorbed energy is sensitive. **Figure 13** shows SEM images of fracture surface at the notch root area at $3.64\times10^{-2}\mathrm{s}^{-1}$ and $203\times10^{-2}\mathrm{s}^{-1}$ in Fig. 11. In Fig. 13(a), dimple patterns are observed at notch root. On the other hand, in Fig. 13(b), dimple is not observed anymore at the notch root. As shown by the arrow in Fig. 6(b), ductile fracture surface ratio is 0% above the critical strain rate of $2.5\times10^{-1}\mathrm{s}^{-1}$. From Fig. 12(a), it is seen that $\sigma_{b,max}$ starts decreasing at $\dot{\varepsilon}$ of $2.5\times10^{-1}\mathrm{s}^{-1}$. This critical strain rate for $\sigma_{b,max}$ is closely related to the presence of dimple pattern at notch root. The notch-bend strength $\sigma_{b,max}$ slightly decreases over critical strain rate where the dimple fracture completely disappears.

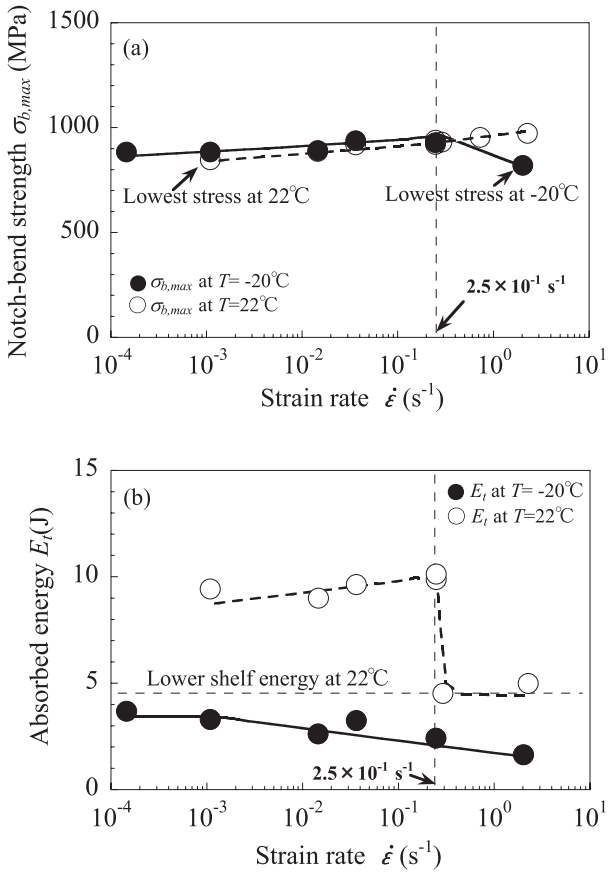

Fig. 12. Effect of strain rate on the notch-bend strength (a) and absorbed energy (b) at temperature T=22°C and −20°C for SSFDI500.

3.4. Comparison with Conventional Ductile Cast Irons on Notch-bend Strength

As stated earlier, from Table 2, it is seen that tensile strength of JIS-FCD500 is similar to that of SSFDI500, which is around 540 MPa. 0.2% proof stress of JIS-FCD700 is similar to that of SSFDI500, which is about 400 MPa. These conventional ferrite-pearlite type ductile cast irons are widely used for industrial applications at room temperature. For example, automotive underbody components, construction machinery components, hydraulic components. **Figure 14** shows transition curves of Charpy absorbed energy E_c to compare with JIS-FCD500, JIS-FCD700 and SSFDI500. It is seen that E_c of JIS-FCD500 (from 10 to 13 J) starts dropping at critical temperature 0°C for upper shelf region, and finally reaches to 4 J at −40°C. This critical temperature

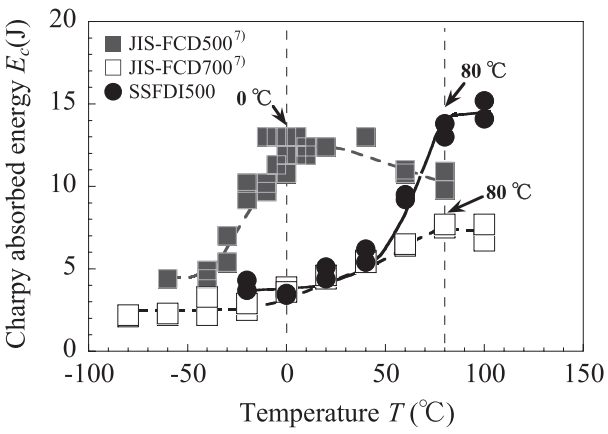

Fig. 14. Results of Charpy impact test for JIS-FCD500, JIS-FCD700 and SSFDI500.

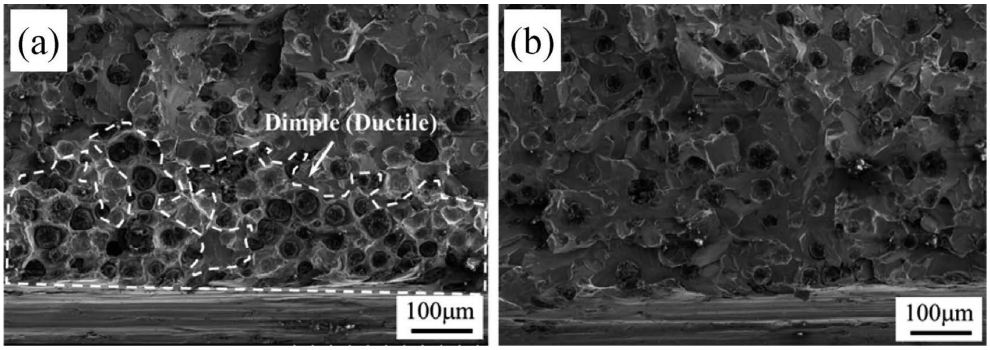

Fig. 13. The comparison of fracture surface of specimen at vicinity of notch root between $\dot{\varepsilon}=3.64\times10^{-2}\mathrm{s}^{-1}$ (a) and $\dot{\varepsilon}=203\times10^{-2}\mathrm{s}^{-1}$ (b) specimens.

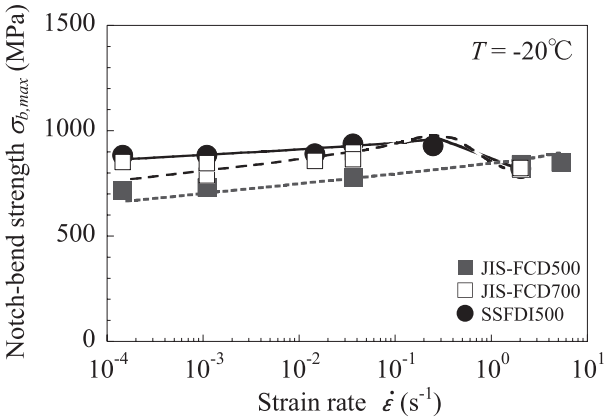

Fig. 15. Effect of strain rate on the notch-bend strength at temperature T=−20°C for JIS-FCD500, JIS-FCD700 and SSFDI500.

of 0°C is lower than that of SSFDI500 (80°C). However, E_c of JIS-FCD700 (about 7 J) starts dropping at 80°C, and finally reaches to about 2.5 J below −20°C. JIS-FCD700 and SSFDI500 have same critical temperature. It is known that higher pearlite ratio raises the ductile-brittle transition temperature in Charpy impact test.[8] The pearlite ratio of JIS-FCD700 is 35% higher than that of JIS-FCD500. Therefore, it is conjectured that JIS-FCD700 and SSFDI500 have almost same critical temperature for upper shelf energy. **Figure 15** shows the relationship between notch-bend strength $\sigma_{b,max}$ and $\dot{\varepsilon}$ on the three-point bending test at −20°C for JIS-FCD500, JIS-FCD700 and SSFDI500. It is seen that all materials have almost the same lowest $\sigma_{b,max}$, which is around 800 MPa, in the range of $\dot{\varepsilon}$, 1.5×10^{-4}~2.0×10^{0}s^{-1}. It is important that the lowest $\sigma_{b,max}$ of SSFDI500 is not so different from that of conventional ductile cast irons even at −20°C when we consider the application of SSFDI500.

4. Conclusions

In this study, the notch-bend strength $\sigma_{b,max}$ was mainly discussed in order to use high Si ductile cast iron SSFDI500 in structures. This material has attracted a lot of attention recently because of smaller section sensitivity and higher fatigue strength. Dynamic three-point bending tests were conducted in the range of stroke speed, 10^{-3}~10^{2} mm/s, at −20~22°C. The conclusions can be made the following way.

(1) The notch-bend strength $\sigma_{b,max}$ is insensitive to both strain rate $\dot{\varepsilon}$ and temperature T. The high Si ductile cast iron has wide industrial application potentiality because $\sigma_{b,max}$ does not decrease in the wide range of $\dot{\varepsilon}$ and T.

(2) Although the absorbed energy E_t decreases with increasing $\dot{\varepsilon}$ and decreasing T, it should be noted that facture does not happen if applied stress does not exceed the strength $\sigma_{b,max}$ which is insensitive to both $\dot{\varepsilon}$ and T. In this sense, the notch-bend strength is more useful than the absorbed energy for structural design of SSFDI500.

(3) The notch-bend strength $\sigma_{b,max}$ does not decrease with increasing $\dot{\varepsilon}$ as far as the fracture origin is ductile even though the absorbed energy E_t is shifted to the lower shelf region.

(4) The lowest strength $\sigma_{b,max}$ obtained at $\dot{\varepsilon}=2.0\times10^{0}$ s^{-1} under T=−20°C is almost equal to the lowest strength $\sigma_{b,max}$ obtained at $\dot{\varepsilon}=1.1\times10^{-3}$ s^{-1} under T=22°C as shown in Fig. 12(a). In other words, $\sigma_{b,max}$ is insensitive to T as well as $\dot{\varepsilon}$.

(5) The lowest strength $\sigma_{b,max}$ of SSFDI500 is almost equal to the lowest strength $\sigma_{b,max}$ of conventional ferrite-pearlite type ductile cast irons in the range of $\dot{\varepsilon}$, 1.5×10^{-4}~2.0×10^{0}s^{-1}, at T=−20°C. These conventional ductile cast irons are used in wide industrial fields and therefore highly reliable.

REFERENCES

1) S. Harada and T. Kobayashi: Kyujyokokuen-Chutetu no Kyodo Hyoka, AGNE Gijyutu-Ctnter, Tokyo, (1999).
2) H. Nakae: Shinpan Chutetu no Zaishitu, Japan Foundry Engineering Society, Tokyo, (2012).
3) R. Larker: *China Foundry*, **6** (2009), 343.
4) R. Larker: Proc. NEWCAST Forum, Bundesverband der Deutschen Gießerei Industrie, Düsseldorf, (2011), 29.
5) H. Löblich: Proc. Deutscher Gießereitag 2013 und 5. NEWCAST Forum, Verein Deutscher Giessereifachleute, Düsseldorf, (2013), 14.
6) EN 1563: 2011, Founding-Spheroidal graphite cast irons.
7) T. Umetani, T. Ikeda, N. Sura, K. Ashizuka, T. Nemoto, H. Takada and K. Ogi: *J. JFS*, **86** (2014), 36.
8) T. Okumoto and T. Aizawa: *Imono*, **35** (1963), 670.
9) K. Nagai, K. Kishitake and T. Owadano: *Imono*, **58** (1986), 350.
10) H. Nagayoshi, H. Yasuda and K. Imanishi: *J. JFS*, **68** (1996), 506.
11) N.-A. Noda, H. Ohtsuka, M. Ando, Y. Sano, Y. Takase, T. Shinozaki and W. Guan: *Trans. Jpn. Soc. Mech. Eng.*, **79** (2013), 1182.
12) M. Ando, N.-A. Noda, Y. Kuroshima, Y. Ishikawa and H. Takeda: *Trans. Jpn. Soc. Mech. Eng.*, **80** (2014), 149.
13) N.-A. Noda, H. Ohtsuka, H. Zheng, Y. Sano, M. Ando, T. Shinozaki and W. Guan: *Fatigue Fract. Eng. Mater. Struct.*, **38** (2015), 125.
14) JIS-G5502: 2001, Spheroidal graphite iron castings.
15) JIS-Z2241: 2011, Metallic materials-Tensile testing-Method of test at room temperature.
16) JIS-Z2242: 2005, Method for Charpy pendulum impact test of metallic materials.
17) H. Yamamoto, T. Kobayashi and H. Fujita: *J. JFS*, **72** (2000), 107.
18) R. Sandstrom and Y. Bergstrom: *Met. Sci.*, **18** (1984),177.
19) N. Sugiura, T. Kobayashi, I. Yamamoto, S. Nishido and K. Hayashi: *J. Jpn. Inst. Light Met.*, **45** (1995), 638.
20) K. Matsugi, G. Bando, G. Sasaki and O. Yanagisawa: *J. JFS*, **79** (2007), 229.
21) T. Kobayashi, H. Matsubara and Y. Ueda: *Tetsu-to-Hagané*, **69** (1983), 1183.
22) S. Nunomura and M. Nakashiro: *Tetsu-to-Hagané*, **64** (1978), 860.
23) T. Nobuki, T. Shiota and M. Hatate: *J. JFS*, **75** (2003), 749.
24) T. Nobuki, T. Shiota and M. Hatate: *J. JFS*, **76** (2004), 555.